[CANCER RESEARCH 62, 7118–7123, December 1, 2002]

A Novel Vascular Endothelial Growth Factor Heparin-binding Domain Substructure Binds to Glycosaminoglycans *in Vivo* and Localizes to Tumor Microvascular Endothelium[1]

Amr El-Sheikh,[2] Cheng Liu, Haining Huang, and Thomas S. Edgington[2]

Department of Immunology, The Scripps Research Institute, La Jolla, California 92037

ABSTRACT

Vascular endothelial growth factor has an exon 7-encoded heparin-binding domain. To explore the expression of complementary ligands on endothelial surfaces *in vivo* and to assess potential for localization within the vascular tree, we introduced a truncated version of this domain (HBDt) into a modified M13 phage. Despite the small size and trace-level expression, this HBDt endowed the phage with affinity for heparin to which it bound *in vitro*. It also preferentially and selectively localized the phage *in vivo* to vascular endothelial surfaces, especially of tumors. Competition assays demonstrated that accumulation and localization of this phage was attributable to expression of the HBDt on the phage surface and sequence comparison suggests its novelty. We propose to use this novel HBDt structure to explore the expression of the ligand glycosaminoglycans within the vascular tree. This structure may facilitate directed delivery of therapeutic molecules.

INTRODUCTION

VEGF[3] is a potent mitogen for ECs and a prime regulator of angiogenesis and vasculogenesis. It induces EC proliferation, promotes cell migration, and inhibits apoptosis. The five known VEGF isoforms, which result from alternative splicing of a single gene, differ in molecular mass, receptor specificity, and binding to cell-surface receptors. VEGF isoforms 165, 189, and 206 contain a HBD (1) for which the structure has been reported (2). These VEGF isoforms bind to two tyrosine-kinase receptors, VEGFR-1 (flt-1) and VEGFR-2 (KDR/flk-1), which are expressed almost exclusively on ECs. $VEGF_{165}$ binds to VEGFR-1 and VEGFR-2 on EC and several non-EC and to novel receptors on tumor-derived cell lines (3). This binding to the M_r 120,000 and M_r 130,000 lower affinity $VEGF_{165}$ receptors is mediated mainly by the exon 7-encoded HBD domain, absent in $VEGF_{121}$. Deletional analysis has localized the activity of the HBD domain to a core substructure within the COOH-terminal 23 amino acids. This HBD substructure inhibited binding and mitogenic activity of $VEGF_{165}$ for human umbilical vein-derived EC and tumor cells *in vitro* (4). Sequence comparison of this HBDt to those of known HBDs indicates novelty and has suggested use of HBDt to explore the distribution of the targets on endothelium and the potential for integration of this structural element into therapeutic proteins.

To explore the expression of complementary molecular targets on the endothelial surface *in vivo* and to assess the potential of this HBDt to localize in a positionally selective manner within the vascular tree, we introduced the HBDt structure, with the following cysteine, into a second geneVIII-modified M13 phage. We established the proper expression of HBDt on the surface of phage through its ability to confer binding to heparin matrix. Phage expressing the entire 24 amino acid residues, with the required cysteine residues, bound heparin with high affinity. We examined the ability of this genetically engineered phage carrying HBDt to bind GAG-deficient mutant cell lines *versus* their wild-type counterparts. In addition, we infused phage into experimental mouse and rat tumor models to investigate whether the HBDt-bearing phage preferentially localizes to the endothelium of certain organs, especially tumors. The phage was found to preferentially accumulate *in vivo* in mouse and rat tumors. Confocal microscopy of tumors and other organs demonstrated that the HBDt.Phage had docked on tumor microvascular ECs in contrast to other tissues.

MATERIALS AND METHODS

HBDt Subdomain Construction. For $VEGF_{165}$ HBDt construct generation, the following two oligonucleotides were annealed and extended. The sequence for 5′ oligonucleotide was 5′-ACAGCGAT*AGCTAGC*GTAGCTCAGGCCGGTTGCTCTTGCAAGAACACGGACA**G**CCGTTGTAAAGCTCGCCAACTGGAACT-3′; and that for 3′ oligonucleotide was 5′-CACGTATCG*AAGCTT*GAGATCCGCC**A**C**A**ACGGCAGGTTCGCTCATTAAGTTCCAGTTGGCGAGCTTTACAACGGCTGTCC-3′. The *Nhe*I and *Hin*dIII restriction sites are underlined. Additional mutant forms were created and analyzed. Replacement of G (bold) with A was used to generate Ser8→Asn and replacement of A (bold) with C was used to generate the Cys24→Gly substitution. The fragment was inserted into the vector (Fig. 1 legend). High fidelity Platinum Pfx DNA polymerase (Invitrogen Corp., Carlsbad, CA) was used for PCR amplification (20 cycles: 94°C, 30 s, 55°C, 15 s, and 72°C, 1 min). Reagents were from New England Biolabs (Beverly, MA).

Heparin Binding. Heparin matrix beads (Sigma, St. Louis, MO), 10% (v/v) in 0.2 M NaCl and 20mN Na_2HPO_4 (pH 7.2) were mixed with phage (10^{10} pfu) with agitation at room temperature for 1 h, centrifuged briefly to precipitate the beads with bound phage, and washed with saline. To elute phage from the beads, 1.2 M NaCl (pH 7.2) was added, and the mixture was incubated with agitation at room temperature for 5 min, then separated by centrifugation. The supernatant fraction containing the phage was collected. The elution step was repeated once, and the eluted phage fractions were combined, then phage was titered by plaque assay. For competitive assays (HBDt.Phage: insertless phage at ratio1:1), the plaque assay was performed in the presence of IPTG and X-Gal (5).

Microscopy. Tissues were embedded in Tissue-Tek ornithine carbamyl transferase (Sakura Finetechnical, Ltd., Tokyo, Japan), frozen, and 5-mm sections were mounted on positively charged slides (Fisher Scientific, Tustin, CA). Sections were fixed in cold acetone for 30 s, blocked with 1:10 goat serum (30 min), washed at room temperature in saline, and blocked with avidin followed by biotin (Avidin/Biotin kit; Vector Labs, Burlingame, CA) for 15 min. Primary rabbit anti-fd bacteriophage (Sigma) and biotin-antimouse or antirat CD31 antibodies were followed by FITC-labeled goat antirabbit immunoglobulin [BD Biosciences PharMingen, La Jolla, CA and Streptavidin Texas Red (Vector Labs)]. Antibodies (1:300) were incubated with sections for 30 min, washed with saline, and mounted in Slow-Fade (Molecular Probes, Eugene, OR).

Cells. To analyze HBDt.Phage binding to GAG-expressing cells, cell lines CHO-pgsA-745 and CHO-K1 representing GAG-deficient cells and their wild-type GAG-positive counterpart (6), respectively, were grown at 37°C, 5% CO_2, in complete media (high glucose DMEM, 10% FBS, glutamine, and nonessential amino acids for CHO-K1 and mixed 1:1 with Kaighn's Nutrient Mixture F-12 for growth of CHO-pgsA-745 cells). Cells were washed with

Received 4/5/02; accepted 10/4/02.

The costs of publication of this article were defrayed in part by the payment of page charges. This article must therefore be hereby marked *advertisement* in accordance with 18 U.S.C. Section 1734 solely to indicate this fact.

[1] This work was supported by NIH Grant P01 HL 16411. A. E-S. is a recipient of NIH Training Grant (Public Health Service Award) T32 CA 75924.

[2] To whom requests for reprints should be addressed, at E-mail: ammor@scripps.edu or tse@scripps.edu.

[3] The abbreviations used are: VEGF, vascular endothelial growth factor; VEGFR, VEGF receptor; EC, endothelial cell; HBD, heparin-binding domain; HBDt, truncated HBD sequence; IPTG, isopropyl-1-thio-β-D-galactopyranoside; X-Gal, 5-bromo-4-chloro-3-indolyl-β-D-galactopyranoside; GAG, glycosaminoglycan; FGF, fibroblast growth factor; FGFR, FGF receptor.

saline, fixed in 4% formaldehyde for 2 min, then incubated 1 h with phage. The cells were washed, and bound phage were visualized with rabbit anti-fd followed by FITC-labeled antirabbit immunoglobulin as above.

Animals. Two animal tumor models were used, syngeneic CT26 colon adenocarcinoma in BALB/c mice and mammary adenocarcinoma MATB-III in Fischer 344 rats. Both cell lines were cultured in complete medium, and $1–3 \times 10^5$ cells were injected s.c. in the back. When tumors were 1–2 cm in diameter, the animals were given injections by tail vein with phage ($\sim 10^{10}$ pfu/mouse and $\sim 10^{11}$ pfu/rat) in saline. After the selected circulation time, the animals were perfused with saline (Invitrogen Corp.), and organs were harvested for plaque assay and histology. All studies have been reviewed and approved by the Institutional Animal Care and Use Committee at The Scripps Research Institute, conducted in TSRI facilities accredited by American Association for the Accreditation of Laboratory Animal Care (AAALAC), with an assurance from the Public Health Service, registered with the United States Department of Agriculture and in compliance with regulations.

RESULTS

HBDt.Phage and Heparin Binding. HBDt DNA (Fig. 1*A*) was cloned into the synthetic geneVIII cassette of the vector (5), which directed low level expression ($\sim$4 copies/phage) of the HBDt peptide-gpVIII. To validate the functional property of the HBDt.Phage, we demonstrated that this phage (VhbdCSC, Fig. 2*A*) binds well to heparin matrix beads; and binding was significantly (>37-fold, $P < 0.05$) greater than wild-type phage lacking the HBDt insert or AL4–15 phage expressing an irrelevant insert. Although the substitution of Ser8 with Asn (VhbdCNG) did not affect binding affinity, the substitution of Cys24 with Gly (VhbdCSG) resulted in binding affinity decline to only $\sim$10-fold more than control wild-type phage. This is consistent with a contribution of Cys24 and formation of this disulfide bridge in the HBDt subdomain of $VEGF_{165}$. The predicted three-dimensional structure (Fig. 1*B*) leaves Cys1 free and disulfide bridges between Cys3 and Cys22 and Cys10 to Cys24. Cys1 appears necessary for functional activity (2), whereas we here demonstrate that the Cys10 to Cys24 bond is also required for optimal heparin affinity. The ability of HBDt.Phage (VhbdCSG) to competitively bind to heparin matrix beads when mixed with wild-type phage is illustrated in Fig. 2*B*, further supporting the role of HBDt. The affinity of the HBDt.Phage with Cys24→Gly replacement (VhbdCSG), al-

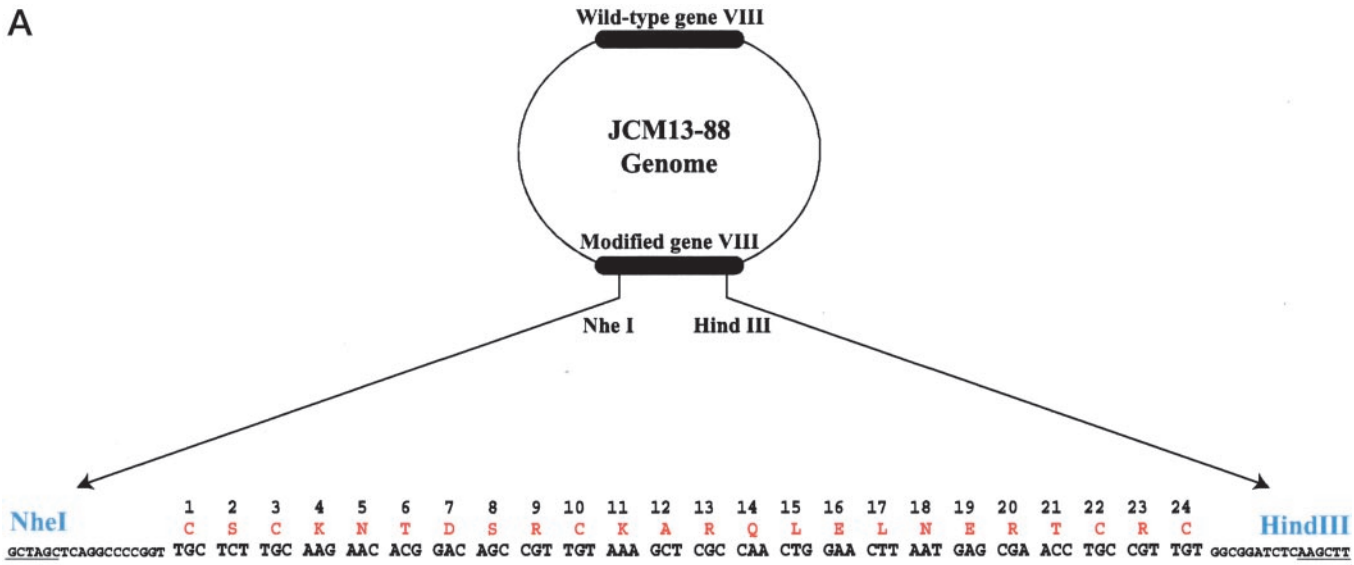

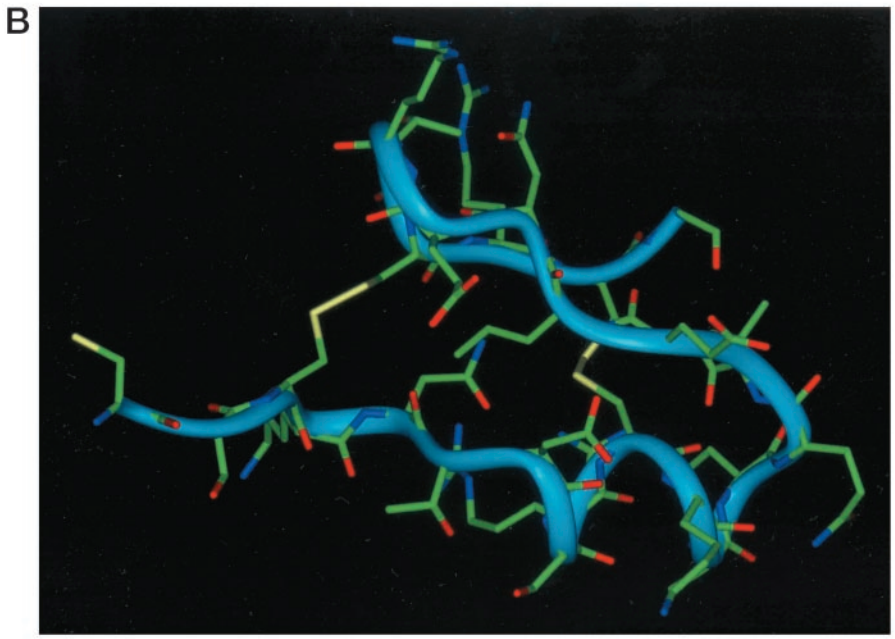

Fig. 1. *A*, construction of geneVIII-HBDt fusion insertion into M13 phage genome. The DNA sequence of the $VEGF_{165}$ HBDt (Cys137 to Cys160 (1)) was generated from synthetic oligonucleotides representing the 5′- and 3′-sequences with an overlap in the middle and adapter sequences containing *Nhe*I and *Hin*dIII restriction sites (*underlined*) at the respective ends. The oligonucleotides were hybridized and the sequence was extended using PCR technology. The restriction-digested HBDt insert and the CIAP-treated vector were gel-purified, ligated, and transformed into *Escherichia coli* XL1-blue. M13 phage plaque assay was performed in the presence of IPTG and X-Gal. Replicative form DNA was prepared from colorless plaques, and the desired DNA constructs were identified by PCR amplification, restriction digest analysis, and DNA sequencing. *B*, predicted structure of the HBDt subdomain. Using the structure solution for the complete HBD domain (2), the truncated form was subjected to computational prediction by molecular dynamics using Discover and energy minimization in InsightII.

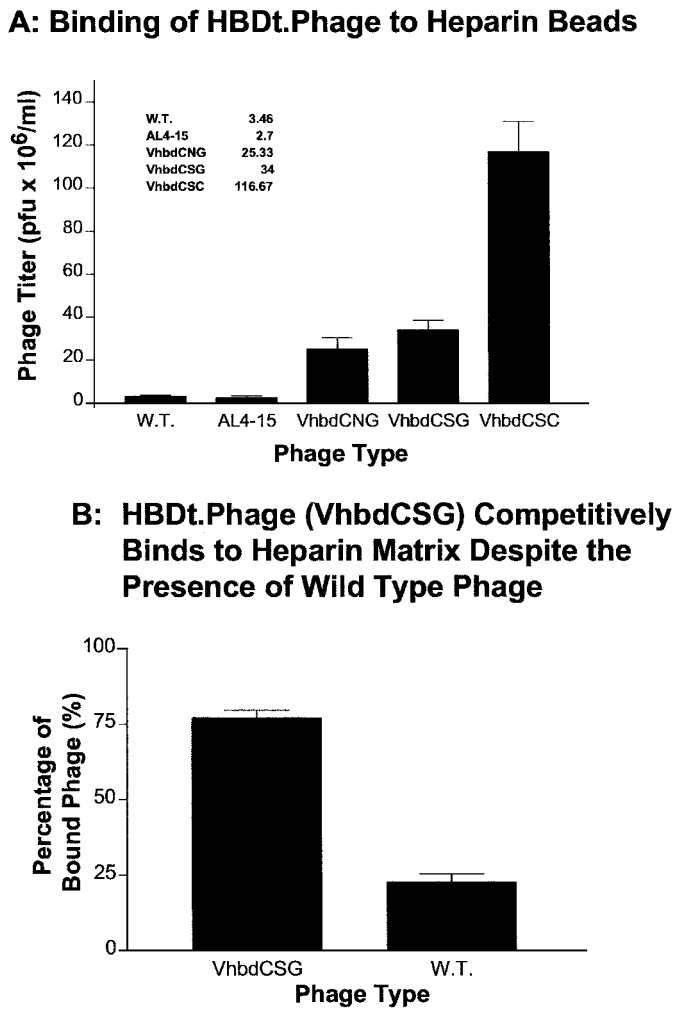

Fig. 2. HBDt.Phage Binds to Heparin Matrix. *A*, equal quantities of HBDt.Phage (VhbdCSC), wild-type (insertless) phage, or irrelevant control (AL4-15) M13 phage were each mixed separately with heparin matrix beads. Two additional mutant forms of HBDt.Phage were created and analyzed. One has a transversion of T to G at codon Cys24 to encode Gly in place of Cys (VhbdCSG). The second has the additional change of G to A at codon 8 to encode Asp in place of Ser8 (VhbdCNG). The binding of the correct HBDt.Phage VhbdCSC to heparin beads was significantly greater (>37-fold) than the control wild-type insertless phage or the irrelevant AL4-15 phage. However, when Cys24 was mutated to Gly in VhbdCSG and this as well as the Ser8→Asp mutation in VhbdCNG, heparin binding decreased to only ~10-fold greater than control phage. Results are from three independent experiments (mean ± SE). Differences between experimental groups were significant by nonparametric one-way ANOVA, Kruskal-Wallis statistics ($P < 0.02$), and by Dunn's Multiple Comparison post tests. *B*, the graph illustrates analysis of competitive binding of HBDt VhbdCSG phage to heparin beads. HBDt VhbdCSG phage was mixed with wild-type phage at 1:1 ratio, and the quantity of phage bound to the heparin beads was assayed. In these experiments, the wild-type phage was quantitated by X-Gal substrate blue conversion. The HBDt.Phage was not competed by irrelevant wild-type phage and composed of 77% of total phage recovered from the heparin matrix.

though diminished relative to HBDt.Phage (VhbdCSC), does retain 77% binding to the heparin matrix and thus residual heparin affinity. These observations are consistent with a role for the constrained three-dimensional structure of this subdomain for full heparin-binding in contrast with the less specific motifs or the assignment of heparin affinity to multiple Arg residues alone (7).

HBDt.Phage Binding to GAGs. HBDt.Phage (VhbdCSC) binding to cell surface GAGs was analyzed by incubation with wild-type CHO-K1 or with CHO-pgsA-745 cells, a CHO mutant disabled for GAG biosynthesis by mutational inactivation of xylosyl transferase (6). Bound phage were visualized by confocal microscopy using FITC fluorescence. Fig. 3*A* shows binding of HBDt.Phage to CHO-K1 cells, whereas there was no binding to GAG-deficient CHO-pgsA-745 cells (Fig. 3*B*), indicating that binding of HBDt is to cell surface GAGs on CHO-K1 cells. To differentiate whether or not the binding of HBDt.Phage to CHO-K1 cells was directly attributable to HBDt on the inserted minimally expressed gpVIII-fusion protein, an irrelevant phage (DB3.Phage) was added to both cell lines. Fig. 3, *C* and *D*, shows that DB3.Phage bound neither cell type, regardless of GAG cell surface expression, further supporting that binding of HBDt.Phage to CHO-K1 cell lines can be attributed to HBDt on the phage surface.

***In Vivo* Biodistribution of HBDt.Phage.** HBDt.Phage was infused i.v. in CT26 tumor-bearing BALB/c mice and in MATB-III tumor-bearing Fisher 344 rats. At selected times thereafter, perfusion of the entire vasculature was performed and tissues were harvested and assayed for phage. Figs. 4, *A* and *C*, show the recovery of phage at 30 and at 60 min. The HBDt.Phage progressively increased in tumors, although no significant increase of phage content was observed for other organs beyond 30 min. Accumulation of HBDt.Phage in tumors was significantly greater ($P < 0.05$) than in organs such as brain and heart. The lung was also analyzed for phage titer in the mouse model and yielded very low titer comparable with that of the heart (data not shown). In addition, CT26 and MATB-III tumors contained 3-fold and 5-fold more phage than spleen and liver, respectively.

The rate of clearance of phage from blood was similar for both animal models with decline of titer from ~20% to ~0.2% of the amount injected, after 30 and 60 min of circulation, respectively (Fig. 4, *B* and *D*). After 60 min, most phage has been cleared from the circulation, and the phage retained in tissues are presumed to result from selective association with targets on the vascular surfaces or phagocytosis in the liver and spleen. It is of interest to note that the increase of phage in CT26 mouse tumors between 30 and 60 min was less than for MATB-III tumors. This may reflect greater expression of HBDt targets in the MATB-III tumor microvasculature.

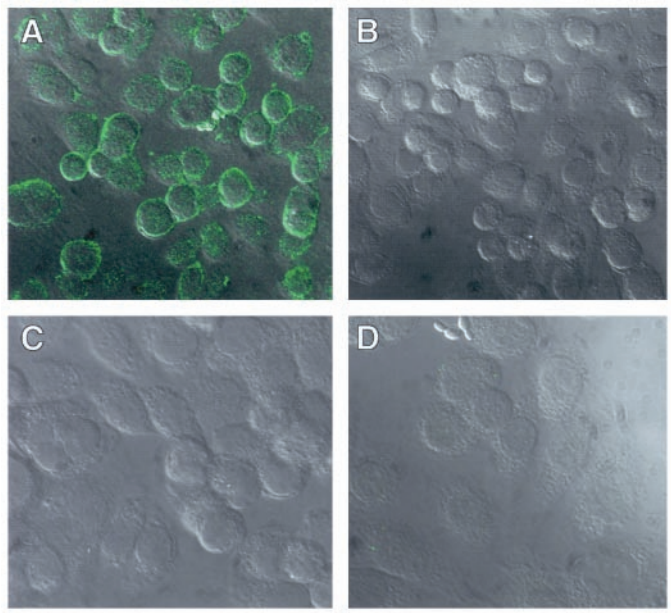

Fig. 3. Binding of HBDt.Phage to cellular GAGs. CHO-k1 cells normally expressing surface GAGs (*A* and *C*), and CHO-GAG-deficient cells pgsA-745 (*B* and *D*) adherent to plastic culture plates were briefly fixed with paraformaldehyde, washed, and overlaid with equal amounts of HBDt.Phage (*A* and *B*) and control DB3.Phage (*C* and *D*). After 60 min, the plates were thoroughly washed with saline and cell-bound phage was visualized with antiphage antibody followed by FITC-conjugated antirabbit IgG antibody (*green*). The signal visualized at 488 nm in the confocal microscope was superimposed over the DIC image of the cells (gray).

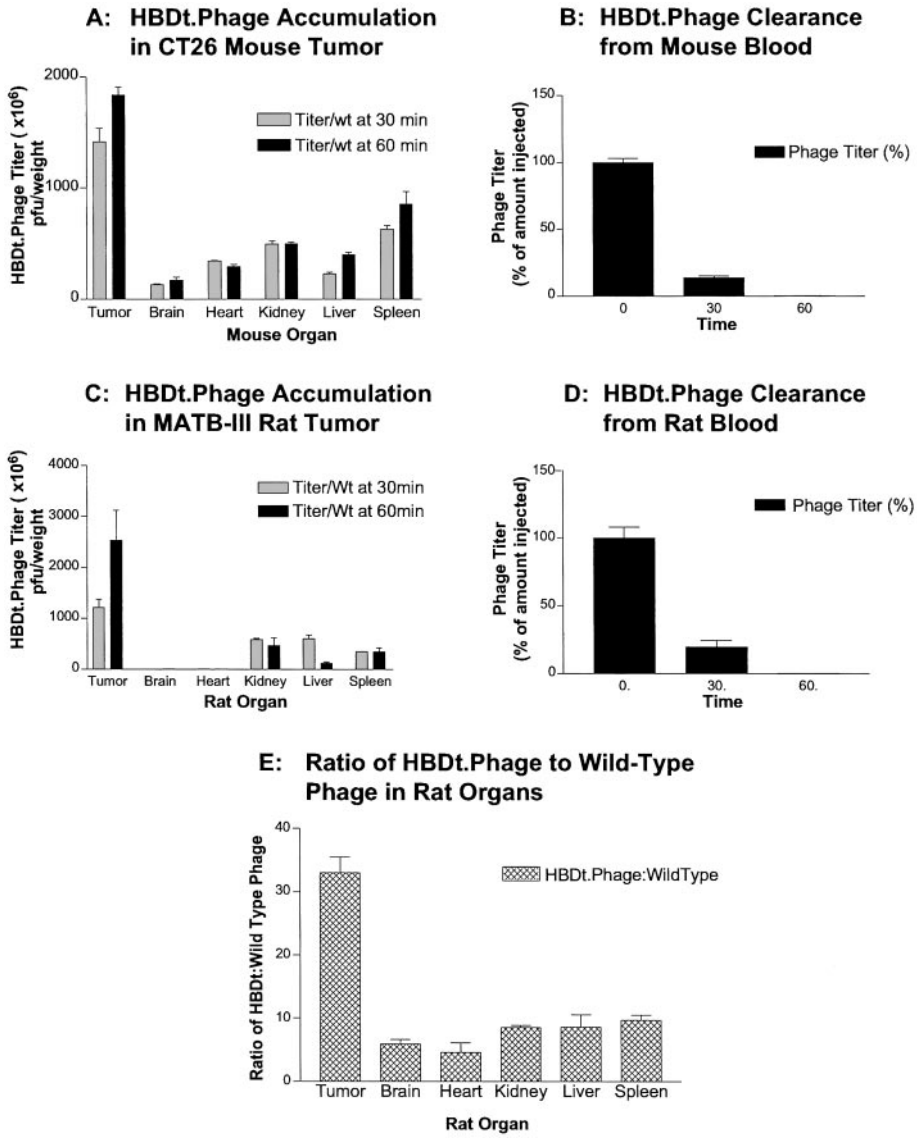

Fig. 4. HBDt.Phage selectively accumulates in CT26 and MATB-III tumors. HBDt.Phage was infused in the tail vein of BALB/c mice (*A*) bearing CT26 tumors and Fischer 344 rats (*C*) with MATB-III tumors. The animals were sacrificed 30 or 60 min later by perfusion with saline at arterial pressure with saline. The organs and tumors were harvested, weighed, and assayed for phage content. The graph shows data at 30 and 60 min. No phage was detected after 3-h circulation (data not shown). Each column represents the mean of three different experiments (mean ± SE). The differences among the experimental groups were found statistically significant using nonparametric one-way ANOVA, Kruskal-Wallis statistics ($P < 0.01$), with Dunn's Multiple Comparison as post tests. The phage titer in the blood was also assayed after 30 and 60 min in mouse (*B*) and rat (*D*). Also, HBDt.Phage was mixed with the wild-type counterpart at 1:1 ratio and infused in Fischer 344 rats carrying MATB-III tumors and left to circulate for 60 min, after which the animals were rapidly perfused with saline at arterial pressure and sacrificed. The graph illustrates the ratio MAT HBDt.Phage to the wild-type insertless phage in different organs. Differentiation between the HBDt.Phage and wild-type phage was based on white *versus* blue plaque generation, respectively. Each column represents the mean and SE of three independent experiments. The differences between groups were significant by nonparametric one-way ANOVA, Kruskal-Wallis statistics ($P < 0.05$), with Dunn's Multiple Comparison post tests.

HBDt.Phage Accumulation Is Mediated by the HBDt Domain. To examine whether accumulation of the HBDt.Phage in these tumors was mediated by the fused HBDt domain on the phage surface, HBDt.Phage was mixed with an equal number of counterpart phage lacking HBDt, and the mixture was infused in MATB-III tumor-bearing rats and allowed to circulate for 60 min, after which the vasculature was perfused. Fig. 4*E* shows the observed ratio of HBDt.Phage to wild-type phage (white/blue) plaque titer obtained for the MATB-III tumors was ~33:1, indicative that preferential accumulation of HBDt.Phage in the tumors required the presence of the HBDt domain on the HBDt.Phage surface, although only present at ~1 copy/phage. This 33:1 ratio in the tumor was significantly ($P < 0.05$) greater than in heart (5.9) or brain (4.6). A ratio of ~9:1 was observed for kidney, liver, and spleen indicative of selective accumulation in these organs as compared with the control phage, although less than in tumor.

Local Docking of HBDt.Phage on Vascular Endothelium. To determine whether the preferential accumulation of HBDt.Phage in some tissues results from physical association with the endothelial surfaces, confocal microscopy with dual immunofluorescence was used to visualize phage and CD31-positive ECs (Fig. 5*A*). In MATB-III tumor-bearing rats, the injected HBDt.Phage was found in the tumor microvasculature mostly colocalized with CD31-positive ECs (Fig. 5*A*). A few phage were observed free in the vascular lumens, presumably a failure to completely washout all blood and phage, an interpretation supported by the occasional erythrocyte aggregates found in a few microvascular channels (Fig. 5*B*).

In contrast to tumors, organs such as brain contained the least HBDt.Phage by plaque assay (Fig. 4*C*), and only very rare phage particles could be found by confocal microscopy (Fig. 5*C*). Of these, none were associated with endothelium. There was moderate accumulation of HBDt.Phage in kidneys; however, these phage were found entirely in glomeruli but not colocalized with CD31-positive endothelium (Fig. 5*E*) and none elsewhere (Fig. 5*G*). Liver and spleen contained phage in hepatic ducts and spleen dendritic follicles (data not shown), the latter appeared to have been phagocytosed during clearance. Similar observations were also observed for the CT26 tumor and mouse tissues (data not shown).

DISCUSSION

The role of VEGF in cancer angiogenesis has been of wide interest and well documented, particularly the $VEGF_{165}$ isoform. The C-proximal aspect of the HBD domain has been shown to significantly

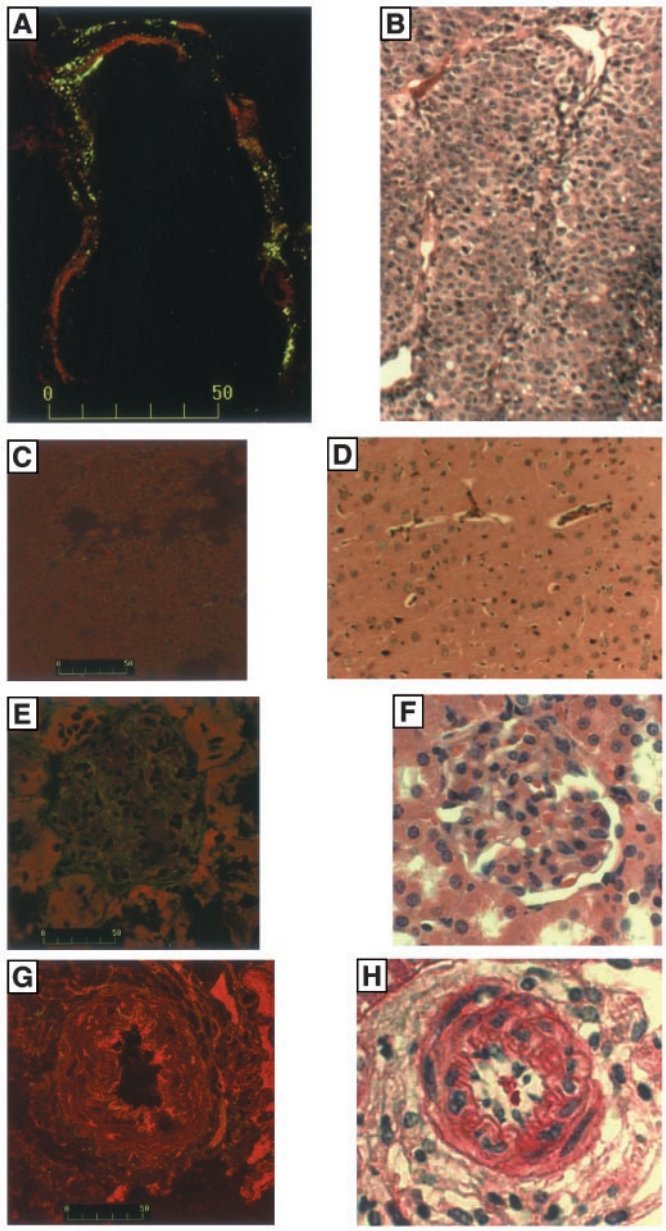

Fig. 5. Localization of the HBDt.Phage *in vivo*. Frozen sections from each of the organs assayed for phage by plaque titer (Fig. 4*C*) were fixed in acetone and incubated with rabbit antiphage IgG followed by a FITC-conjugated antirabbit IgG antibody and also with biotin-conjugated mouse antirat anti-CD31 monoclonal antibody followed by Streptavidin-conjugated Texas Red. The phage-positive signals (FITC) and CD31-positive ECs (Texas Red) were visualized under 488 and 568 nm light by confocal microscopy (power ×63 oil lens, scale shown in μm). *A*, *C*, *E*, and *G* show localization of HBDt.Phage (*green*) with respect to the CD31-positive ECs (*red*) in the MATB-III tumor, brain, kidney glomerulus, and a renal arterial vessel, respectively. *B*, *D*, *F*, and *H* show the H&E stain for adjacent serial sections

inhibit the binding and mitogenic activity of $VEGF_{165}$ for human umbilical vein-derived EC and MDA-MB-231 tumor cells (4). The effect of the HBD domain of VEGF on tumor cell lines is only one reason why it is of interest in regard to angiogenesis and tumor biology. Another is the structural relationship between HBD, the truncated subdomain and other heparin-binding proteins.

Here, the C-proximal substructure of the HBD of $VEGF_{165}$ was investigated for its potential to mediate homing to tumor microvasculature and other tissues. The 23 C-proximal codons of exon 7 with the first codon (for Cys) of exon 8 of $VEGF_{165}$ was prepared as the HBDt DNA and was inserted into a synthetic geneVIII cassette under the control of the *Lac* promoter inserted into the genome of a modified M13 phage vector. This encoded expression of the HBDt peptide fused at the NH_2 terminus of the coat glycoprotein gpVIII but expressed at a very low number. The expression of HBDt on the surface of the phage was increased from ~1 to ~4–7 copies/phage by addition of IPTG and propagation at 25°C (5). HBDt expression on the surface of the phage was confirmed by the binding of HBDt.Phage, and not of control phage, to heparin matrix (Fig. 2*A*) and was reinforced by the ability of HBDt.Phage to competitively bind to heparin-coated beads in the presence of wild-type phage (Fig. 2*B*).

The HBD of the $VEGF_{165}$ receptor, VEGFR-2(KDR/flk-1), has been identified on the extracellular domain (8). The binding of $VEGF_{165}$ to its receptor is thought to occur in a manner similar to that of FGF and its receptor (FGFR), where signal transduction requires association of FGF with both its receptor and heparan sulfate proteoglycans in a complex on the cell surface. Crystallographic studies of the FGF-FGFR complex demonstrate that heparin associates with both receptor and ligand such that two FGF molecules are linked to one FGFR molecule within a functional heteropentamer FGF_2:FGF_2:heparin (9). However, the sequence of the $VEGF_{165}$ HBDt is not homologous to the FGF counterpart or any other recognized heparin-binding motif. Table 1 lists examples of some of the known HBDs found in other protein families. Sequence analysis has identified motifs present in the HBDs from growth factors and adhesion proteins, bone morphogenic proteins (10), axonal guidance molecules (11), viral coat proteins (12–14), coagulation pathway inhibitor protein TFPI (15), and regulatory peptides (16, 17). The majority of motifs adopt the consensus sequences XBBBXXBX or XBBXBX, which were described by Cardin and Weitraub (7).

The HBDt subdomain analyzed here lacks these sequence motifs or close homology to protein motifs in the databases, nor does it contain clusters of basic residues particularly Arg residues. The basic residues of the VEGF HBDt are present in the sequence in a manner distinct from described HBD motifs. Furthermore, the functional activity of the HBDt subdomain is dependent on its three-dimensional structure. The formation of the correct disulfide bridges between Cys3 and Cys22 and between Cys10 and Cys24, as previously predicted (1), was shown here to be important in imposing the correct three-dimensional structure and affinity for heparin (Fig. 2*A*) rather than the number of basic residues in the sequence as previously implicated for other motifs. The structure-function relationship of proteins with heparin is well established for antithrombin-III where a unique carbohydrate structure, a minor subset of heparin, is the cognate ligand that facilitates the interaction of thrombin with antithrombin-III (18).

Selective accumulation of the HBDt.Phage in tumors in mouse and rat models (Fig. 4) is significant. *In vivo* clearance of i.v. administered HBDt.Phage is rapid and proceeds at similar rates in both animal models (Fig. 4, *B* and *D*). Whereas the concentration of phage in the blood rapidly declined within 1 h to ~0.2% of that injected, accumulation of HBDt.Phage in the tumors progressively increased. This was observed only for tumors, and the accumulation of HBDt.Phage was statistically significant compared with organs such as brain and heart.

We suggest that there exists a unique characteristic of tumor microvasculature that is responsible for enhanced localization of $VEGF_{165}$ that is mediated by the HBDt subdomain. Furthermore, microscopic analysis colocalized the phage in the tumor to the CD31-positive endothelial surfaces in both small channels (data not shown) as well as in larger channels (1–5 mm in diameter) where the circulation is more robust (Fig. 5*A*), indicating that suboptimal perfusion of the tumor microvasculature is not responsible for the accumulation of HBDt expressing phage. In fact, HBDt.Phage out-competed its wild-type counterpart in homing to tumor microvascular endothelium (Fig. 5*E*), presumably because of interaction with cell surface GAGs. It was recently reported that

Table 1 *Conventional heparin-binding domains*[a]

Molecule	Group	HBD sequence	Motif
aFGF (17)	GF[b]	PLGNYKKPKLLYCSNG	XBBXBX
bFGF (22)	GF	GHFKDPKRLYCKNGGF	?(XBBXXXBX)
β-TG (23)	GF	PDAPRIKKIVQKKLAG	XBXBBX
FGFR-1 (23)	GF receptor	AAPVAHLKKEMKN	?(XBBXXBX)
Noggin (9)	TGF-β binding protein	AQGKKQRLSKKLRRKLQM	XBBXBX, ?(B)xN
IGFBP-3 (23)	GF binding protein	GFYKKKQCRPSKG	XBBBXXBX
Apo B (23)	Human plasma LDL	FIIPSPKRPVKLLSG	?(XBBXXBX)
Apo B (17)	Human plasma LDL	ALLKKTKNSEEF	XBBXBX
Apo E (23)	Human plasma LDL	SHLRKLRKRLLRDA	XBBBXXBX
Apo E (17)	Human plasma LDL	AWGERLRARMEEMGSRTRDRL	?(XBX)xN
TFPI (14)	Tissue factor pathway inhibitor	GGLIKTKRKRKKQRVKIAY	?(B)xN
PVC-21 MuLV (12)	Murine leukemia virus	PGSHRPRKAKSC	XBBXBX
PRV-Be (11)	Pseudorabies virus	SRRKPPRN. . .YRRGRF	XBBBXXBX, XBBXBX
α^{4N}(V)-NTD (24)	Adhesion molecule	RRRKGKGKKKDRGRKGKG	(XBBXB)x3, ?(B)xN
α4 Type V collagen (24)	Collagen	PRRRKGKGKKKDRGRKGKGRKKNKT	XXBBXBX, ?(B)xN
Laminin α1 (25)	Adhesion molecule	DVRKRLQVQLSIRT	?(XBBBX)
Annexin II tetramer, p36 (23)	Adhesion molecule	LKIRSEFKKKYGKSLYY	XBBBXXBX
Pro-islet amyloid polypeptide (16)	Regulatory peptide	TPIESHQVEKRKCNTATC	?(XBBBX)
Heparin affin regulatory peptide (HARP) (15)	Regulatory peptide	GKLTKPKQAESKKKKKE	?(B)xN

[a] HBDs have been designated by common motifs XBBXBX or XBBBXXBX (17). The ? indicates suggested potential motifs.
[b] GF, growth factor; TGF, transforming growth factor.

tumors such as rat mammary carcinomas contain high levels of mast-cell heparin, which functions as an anticoagulant to modulate hemostasis and blood perfusion in tumors (19). Other targets that are structurally related to heparin such as heparan sulfates or chondroitin sulfates were also recognized by this domain. Current studies in progress identify the target as a chondroitin sulfate-type GAG. Such molecules if associated with the local endothelial surfaces could facilitate HBDt association. The ability of HBDt.Phage to rather preferentially home to tumor microvasculature suggests a potential use of this structure to facilitate association of therapeutic molecules with the tumor microvasculature. As in prior studies, the design of selective tumor vascular thrombogens that initiate local occlusive thrombosis can achieve infarctive eradication of tumors (20). Such designer proteins require a tumor selective vascular association domain to achieve activation of the thrombogenic cascade only in tumors.

The role of heparins and related structures on cell surface GAGs are of increasing interest in unraveling the molecular pathobiology of angiogenesis and cancer metastasis (21). The synthesis of various GAGs by the tumor-associated microvascular endothelium during angiogenesis and thereafter may be important in certain aspects of tumor vascular biology. Elucidation of the targets of the HBDt subdomain remains to be resolved. The novelty of this domain, its role, and the potential for incorporation in design of therapeutic molecules holds promise (22).

ACKNOWLEDGMENTS

We thank Dr. Angray Kang for providing us with the original phage construct. We also thank Dr. Malcolm Wood for his assistance with the confocal microscopy and Barbara Parker for her administrative help and assistance with the manuscript.

REFERENCES

1. Keck, R. G., Berleau, L., Harris, R., and Keyt, B. A. Disulfide structure of the heparin binding domain in vascular endothelial growth factor: characterization of posttranslational modifications in VEGF. Arch. Biochem. Biophys., *344:* 103–113, 1997.
2. Fairbrother, W. J., Champe, M. A., Christinger, H. W., Keyt, B. A., and Starovasnik, M. A. Solution structure of the heparin-binding domain of vascular endothelial growth factor. Structure (London), *6:* 637–648, 1998.
3. Soker, S., Fidder, H., Neufeld, G., and Klagsbrun, M. Characterization of novel vascular endothelial growth factor (VEGF) receptors on tumor cells that bind VEGF165 via its exon 7-encoded domain. J. Biol. Chem., *271:* 5761–5767, 1996.
4. Soker, S., Gollamudi-Payne, S., Fidder, H., Charmahelli, H., and Klagsbrun, M. Inhibition of vascular endothelial growth factor (VEGF)-induced endothelial cell proliferation by a peptide corresponding to the exon 7-encoded domain of VEGF165. J. Biol. Chem., *272:* 31582–31588, 1997.
5. Chappel, J. A., He, M., and Kang, A. S. Modulation of antibody display on M13 filamentous phage. J. Immunol. Methods, *221:* 25–34, 1998.
6. Esko, J. D., Stewart, T. E., and Taylor, W. H. Animal cell mutants defective in glycosaminoglycan biosynthesis. Proc. Natl. Acad. Sci. USA, *82:* 3197–3201, 1985.
7. Cardin, A. D., and Weintraub, H. J. Molecular modeling of protein-glycosaminoglycan interactions. Arteriosclerosis (Dallas), *9:* 21–32, 1989.
8. Dougher, A. M., Wasserstrom, H., Torley, L., Shridaran, L., Westdock, P., Hileman, R. E., Fromm, J. R., Anderberg, R., Lyman, S., Linhardt, R. J., Kaplan, J., and Terman, B. I. Identification of a heparin binding peptide on the extracellular domain of the KDR VEGF receptor. Growth Factors, *14:* 257–268, 1997.
9. Pellegrini, L., Burke, D. F., von Delft, F., Mulloy, B., and Blundell, T. L. Crystal structure of fibroblast growth factor receptor ectodomain bound to ligand and heparin. Nature (Lond.), *407:* 1029–1034, 2000.
10. Paine-Saunders, S., Viviano, B. L., Economides, A. N., and Saunders, S. Heparan sulfate proteoglycans retain Noggin at the cell surface: a potential mechanism for shaping bone morphogenetic protein gradients. J. Biol. Chem., *277:* 2089–2096, 2002.
11. Chong, J. M., Uren, A., Rubin, J. S., and Speicher, D. W. Disulfide bond assignments of secreted Frizzled-related protein-1 provide insights about Frizzled homology and netrin modules. J. Biol. Chem., *277:* 5134–5144, 2002.
12. Flynn, S. J., and Ryan, P. The receptor-binding domain of pseudorabies virus glycoprotein gC is composed of multiple discrete units that are functionally redundant. J. Virol., *70:* 1355–1364, 1996.
13. Jinno-Oue, A., Oue, M., and Ruscetti, S. K. A unique heparin-binding domain in the envelope protein of the neuropathogenic PVC-211 murine leukemia virus may contribute to its brain capillary endothelial cell tropism. J. Virol., *75:* 12439–12445, 2001.
14. Dechecchi, M. C., Melotti, P., Bonizzato, A., Santacatterina, M., Chilosi, M., and Cabrini, G. Heparan sulfate glycosaminoglycans are receptors sufficient to mediate the initial binding of adenovirus types 2 and 5. J. Virol., *75:* 8772–8780, 2001.
15. Mine, S., Yamazaki, T., Miyata, T., Hara, S., and Kato, H. Structural mechanism for heparin-binding of the third Kunitz domain of human tissue factor pathway inhibitor. Biochemistry, *41:* 78–85, 2002.
16. Bernard-Pierrot, I., Delbe, J., Caruelle, D., Barritault, D., Courty, J., and Milhiet, P. E. The lysine-rich C-terminal tail of heparin affin regulatory peptide is required for mitogenic and tumor formation activities. J. Biol. Chem., *276:* 12228–12234, 2001.
17. Park, K., and Verchere, C. B. Identification of a heparin binding domain in the N-terminal cleavage site of pro-islet amyloid polypeptide. Implications for islet amyloid formation. J. Biol. Chem., *276:* 16611–16616, 2001.
18. Rosenberg, R. D., Jordan, R. E., Favreau, L. V., and Lam, L. H. Highly active heparin species with multiple binding sites for antithrombin. Biochem. Biophys. Res. Commun., *86:* 1319–1324, 1979.
19. Samoszuk, M. K., Su, M. Y., Najafi, A., and Nalcioglu, O. Selective thrombosis of tumor blood vessels in mammary adenocarcinoma implants in rats. Am. J. Pathol., *159:* 245–251, 2001.
20. Huang, X., Molema, G., King, S., Watkins, L., Edgington, T. S., and Thorpe, P. E. Tumor infarction in mice by antibody-directed targeting of tissue factor to tumor vasculature. Science (Wash. DC), *275:* 547–550, 1997.
21. Vlodavsky, I., and Friedmann, Y. Molecular properties and involvement of heparanase in cancer metastasis and angiogenesis. J. Clin. Investig., *108:* 341–347, 2001.
22. Ye, S., Luo, Y., Lu, W., Jones, R. B., Linhardt, R. J., Capila, I., Toida, T., Kan, M., Pelletier, H., and McKeehan, W. L. Structural basis for interaction of FGF-1, FGF-2, and FGF-7 with different heparan sulfate motifs. Biochemistry, *40:* 14429–14439, 2001.
23. Kassam, G., Manro, A., Braat, C. E., Louie, P., Fitzpatrick, S. L., and Waisman, D. M. Characterization of the heparin binding properties of annexin II tetramer. J. Biol. Chem., *272:* 15093–15100, 1997.
24. Erdman, R., Stahl, R. C., Rothblum, K., Chernousov, M. A., and Carey, D. J. Schwann cell adhesion to a novel heparan sulfate binding site in the N-terminal domain of α 4 type V collagen is mediated by syndecan-3. J. Biol. Chem., *277:* 7619–7625, 2002.
25. Hoffman, M. P., Engbring, J. A., Nielsen, P. K., Vargas, J., Steinberg, Z., Karmand, A. J., Nomizu, M., Yamada, Y., and Kleinman, H. K. Cell type-specific differences in glycosaminoglycans modulate the biological activity of a heparin-binding peptide (RKRLQVQLSIRT) from the G domain of the laminin α1 chain. J. Biol. Chem., *276:* 22077–22085, 2001.

A Novel Vascular Endothelial Growth Factor Heparin-binding Domain Substructure Binds to Glycosaminoglycans *in Vivo* and Localizes to Tumor Microvascular Endothelium

Amr El-Sheikh, Cheng Liu, Haining Huang, et al.

Cancer Res 2002;62:7118-7123.